Agricultural Ecology and Environment

https://doi.org/10.48130/aee-0026-0002

Original Research

Open Access

Sulfur-ferrihydrite-modified biochar for simultaneous immobilization of arsenic and cadmium in co-contaminated water/soil: performance and mechanisms

Weijie Xu[1], Dong Huang[2], Houbo Huang[2], Bo Zheng[1], Xiaowen Teng[1], Ijlal Ahmad[3], Hanbo Chen[4], Yaqian Li[5] and Dan Liu[1*]

Received: 7 November 2025

Revised: 24 December 2025

Accepted: 15 January 2026

Published online: 28 February 2026

Abstract

Environmental contamination by arsenic (As), and cadmium (Cd) presents a significant remediation challenge due to their distinct chemical speciation, adsorption affinities, and transport behaviors. In this work, a sulfur-ferrihydrite-functionalized biochar (SFB) was engineered as a versatile soil amendment capable of immobilizing both Cd(II), and As(III) simultaneously. Comprehensive characterization confirmed that sulfur species and ferrihydrite nanoparticles were homogeneously distributed across the biochar surface, resulting in a hierarchically porous composite enriched with reactive functional groups and enhanced redox-active interfaces. Adsorption experiments revealed that SFB achieved maximum uptake capacities of 76.69 mg g^{-1} for Cd, and 8.28 mg g^{-1} for As, substantially exceeding those of rice straw biochar (BC), ferrihydrite (FH), and ferrihydrite-modified biochar (FB). The adsorption behavior conformed well to the Langmuir isotherm, and pseudo-second-order kinetic models, suggesting that both physical adsorption and chemical interactions governed Cd(II)/As(III) sequestration. Spectroscopic and microscopic analyses indicated that Cd(II) was immobilized mainly through ion exchange, surface coordination, and the formation of CdS and FeS precipitates. In contrast, As retention proceeded via oxidation of As(III) to As(V), followed by strong inner-sphere complexation with Fe–O functional groups. These coupled redox and coordination processes created synergistic interfacial sites capable of effectively capturing both cationic and anionic contaminants. Soil incubation experiments further confirmed the effectiveness of SFB, showing maximum reductions in bioavailable Cd (32.59%–41.26%), and As (50.06%–64.06%), along with their transformation into more stable residual fractions. Overall, the results demonstrate that SFB represents a promising amendment for the simultaneous stabilization of Cd and As in co-contaminated agricultural soils.

Keywords: Functional biochar, Toxic metal(loid)s, Adsorption mechanisms, Immobilization, Soil remediation

Highlights

- Cd(II) adsorption was driven by ion exchange and co-precipitation, whereas As(III) was controlled by oxidation-complexation.
- Sulfur-ferrihydrite-biochar (SFB) exhibits superior synergistic adsorption toward both Cd(II) and As(III).
- SFB decreases soil Cd/As bioavailability and transforms them into stable residual fractions.

* Correspondence: Dan Liu (liudan@zafu.edu.cn)

Full list of author information is available at the end of the article.

https://doi.org/10.48130/aee-0026-0002

Graphical abstract

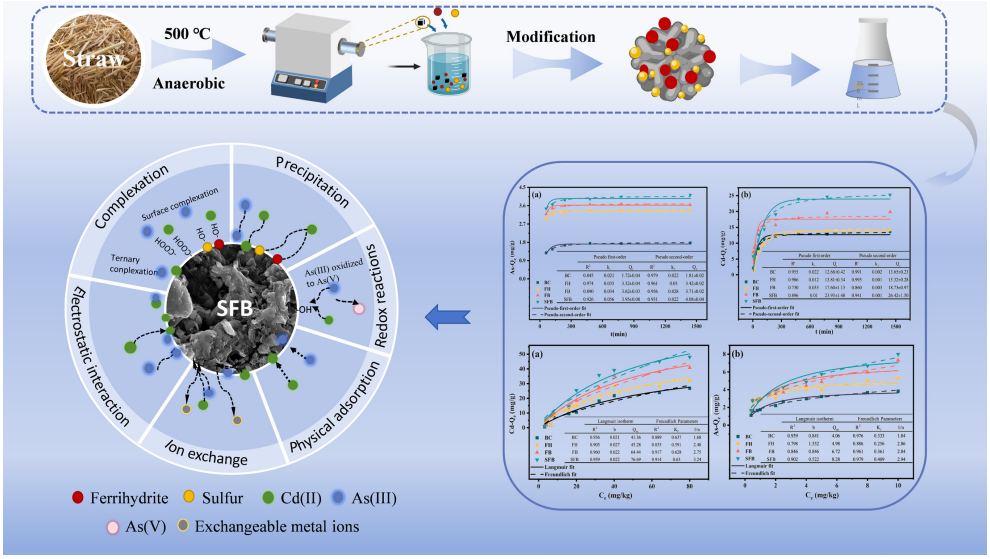

Introduction

Soil contamination by cadmium (Cd), and arsenic (As) has emerged as a critical global environmental issue. These toxic metal(loid)s are predominantly introduced into soils through anthropogenic activities, including mining, smelting, excessive fertilizer application, and irrigation with contaminated water, and are characterized by high mobility and bioavailability[1]. Once introduced into agricultural soils, Cd(II) and As species, primarily As(III) and As(V), can be taken up by crops and transferred through the food chain, thereby posing substantial ecological and human health risks[2]. Long-term exposure to these contaminants has been associated with adverse health outcomes such as renal dysfunction, skeletal damage, and increased carcinogenic risk[3]. In China, more than 2×10^5 km^2 of agricultural land has been reported to be co-contaminated with Cd and As, with particularly severe impacts in southern regions with intensive agricultural activity[4–5]. In paddy soils, where Cd/As co-contamination is widespread, flooded and reducing conditions commonly prevail. Under such low redox potential environments, both microbial and abiotic processes strongly promote the reduction of As(V) to As(III), leading to As(III) becoming the dominant dissolved As species[6]. Compared with As(V), As(III) exhibits markedly higher mobility, bioavailability, and toxicity, and is therefore regarded as the principal contributor to arsenic-related environmental and health risks in submerged agroecosystems[2]. Consequently, recent Fe- and S-based remediation strategies have increasingly focused on targeting As(III), and the present study similarly prioritizes this species to address the most environmentally relevant and risk-dominant form of arsenic in Cd/As co-contaminated soils[7,8].

Remediation of Cd/As co-contaminated soils is particularly challenging because of the contrasting geochemical behaviors of these elements. Cd predominantly occurs as Cd(II), and interacts with negatively charged surfaces through ion exchange, complexation, and precipitation[7]. In contrast, As is mainly present as oxyanionic species ($H_2AsO_3^-$ and $HAsO_4^{2-}$), whose mobility is strongly regulated by soil pH and redox conditions[9]. The simultaneous presence of cationic and anionic contaminants often leads to competitive adsorption and complex redox interactions, thereby limiting the effectiveness of conventional immobilization approaches[3,10]. Therefore, the development of multifunctional amendments capable of concurrently stabilizing both Cd(II) and As(III) remains a critical scientific and practical objective. Biochar is widely used as a soil amendment due to its high surface area, porous structure, and abundant oxygen-containing functional groups that enable effective immobilization of cationic metals[11]. Numerous studies have demonstrated that biochar effectively stabilizes Cd(II) through mechanisms such as electrostatic attraction, ion exchange, and surface complexation[12]. However, pristine biochar, due to its predominantly negative surface charge, limits the adsorption of anionic contaminants such as As[13]. Modification with ferrihydrite can markedly enhance As(III) retention via inner-sphere complexation, while simultaneously improving Cd(II) immobilization through additional ion exchange and surface coordination sites[14–17]. When ferrihydrite is supported on biochar, its dispersion and accessibility are substantially improved, resulting in heterogeneous composites with diverse reactive binding domains[13,18,19]. Such ferrihydrite-modified biochars integrate the strong sorption capacity of ferrihydrite with the structural stability of biochar, leading to enhanced immobilization of both Cd(II) and As(III)[20–22].

Sulfur modification further introduces reactive sulfide species that can promote CdS precipitation and enhance iron redox cycling, thereby strengthening the removal of Cd(II) and As(III)[23]. Although Fe- or S-modified biochars have demonstrated promise, most studies focus on single-metal systems, and only limited efforts have been devoted to integrating Fe and S functionalities within a unified Fe–S–biochar framework[24–26]. For instance, sulfide-modified α-FeOOH has been reported to exhibit nearly threefold higher As(V) adsorption capacity than pristine α-FeOOH, attributed to sulfur-induced activation of Fe sites and enhanced Fe-As coordination[27]. These findings suggest that the incorporation of both sulfur and ferrihydrite into a biochar matrix may yield a multifunctional composite capable of simultaneously stabilizing Cd(II) and As(III) through complementary mechanisms, including precipitation, surface complexation, and redox transformation. However, the mechanistic understanding of how Fe–S coupling affects Cd/As co-immobilization, particularly under competitive and redox-active soil conditions, remains insufficient.

To address these gaps, this study synthesized a sulfur-ferrihydrite-modified biochar (SFB) and systematically evaluated its performance in immobilizing Cd(II) and As(III) in both aqueous and soil systems. The objectives of this study are to: (1) assess the adsorption behavior and capacity of SFB for Cd and As under controlled experimental conditions; (2) elucidate the mechanisms of Cd(II) and As(III) immobilization, including ion exchange, precipitation, oxidation-reduction, and surface complexation processes; and (3) examine the effects of SFB application on the chemical speciation and bioavailability of Cd and As in contaminated soils.

Materials and methods

Preparation and modification of biochar

Biochar preparation

Rice straw was air-dried, cut into pieces, filtered, and passed through a 5-mm sieve prior to pyrolysis. Biochar was produced by slow pyrolysis of rice straw at 550 °C for 2 h under oxygen-limited conditions in a muffle furnace, with a heating rate of 5 °C min^{-1}. After naturally cooling to room temperature, the resulting biochar was thoroughly washed with ultrapure water to remove residual ash and impurities, filtered, and sieved through a 100 mesh. The obtained material was designated as pristine biochar (BC).

Biochar modification

Ferrihydrite was synthesized following the method described by Du et al.[20]. Briefly, 1.5 mol L^{-1} NaOH was added dropwise to a 0.1 mol L^{-1} $Fe(NO_3)_3$ solution until the pH reached 7.0. The suspension was aged for 1 h, after which the supernatant was decanted. The precipitate was separated by centrifugation at 4,500 rpm, washed twice with ultrapure water, and dialyzed in darkness for three days to remove residual Na^+ and NO^{3-} ions. The resulting solid was dried at 60 °C for 8 h, ground, sieved through a 100-mesh screen, and denoted as ferrihydrite (FH). More detailed chemicals and reagents are presented in the Supplementary Material (S1.1 Chemicals and reagents).

To prepare ferrihydrite-modified biochar (FB), BC and FH were mixed at a mass ratio of 2:1, and dispersed in 1 mol L^{-1} KOH solution. The suspension was stirred at 60 °C for 72 h, allowed to settle for 24 h, and centrifuged at 5,000 rpm. The resulting precipitate was washed repeatedly with ultrapure water, frozen at −20 °C overnight, and subsequently freeze-dried.

Sulfur modification was conducted using a CS_2-alkaline reaction system. Briefly, 100 mL of 0.40 mol L^{-1} NaOH solution was reacted with CS_2 at a molar ratio of 1:1.5 under continuous stirring at 25 °C for 4 h, followed by ultrasonication for 1 h to ensure homogeneous dispersion. The mixture was then maintained at 40 °C with magnetic stirring for 16 h, cooled to ambient temperature, and filtered through a 0.45-μm membrane. Under alkaline conditions, this reaction predominantly generates inorganic polysulfides (Na_2S_x) and dithiocarbamate-like species, which act as sulfur donors. Subsequently, 10 g of FB was dispersed in 100 mL of the sulfur-modification solution and stirred at 45 °C for 8 h to facilitate sulfur incorporation. The final product was filtered, dried, sieved through a 100-mm sieve, and designated as sulfur-ferrihydrite-modified biochar (SFB).

Batch adsorption experiments

Batch adsorption experiments were performed at 25 °C to evaluate the adsorption behavior of Cd(II) and As(III) on BC, FH, FB, and SFB. All solutions were adjusted using 0.1 mol L^{-1} NaOH or 0.1 mol L^{-1} HCl, and the experiments were conducted in triplicate. Initial and equilibrium concentrations of Cd(II) and As(III) were quantified using inductively coupled plasma mass spectrometry (ICP-MS, Agilent 7000, Japan).

All amendments were applied at a dosage of 1.5 g L^{-1} unless otherwise specified. Suspensions were agitated at 180 rpm for 24 h. The optimum pH was determined using a binary system containing a 5 mg L^{-1} As(III) and 40 mg L^{-1} Cd(II) solution, with pH values adjusted to 2, 3, 4, 5, 6, 7, 8, and 9.

Dosage-dependent experiments were conducted at amendment dosages of 0.2, 0.5, 1, 1.5, and 2g L^{-1} in a solution containing 40 mg L^{-1} Cd(II) and 5 mg L^{-1} As(III). Kinetic experiments were carried out by sampling at predetermined intervals (5, 10, 30, 60, 120, 240, 360, 540, 720, 960, 1,200, and 1,440 min) from the solution containing 40 mg L^{-1} Cd(II) and 5 mg L^{-1} As(III). All samples were filtered through 0.45 μm membranes, acidified, and analyzed by ICP-MS.

Modeling for metal(liod)s adsorption

Adsorption kinetics were fitted using pseudo-first-order and pseudo-second-order models. Equilibrium adsorption data were analyzed using the Langmuir and the Freundlich isotherm models. Detailed equations, fitting parameters, and characterization data are provided in the Supplementary Material (S1.2 Modeling for metal(liod)s adsorption, S1.3 Characterization of amendments before and after metal(liod)s adsorption).

Pot experiment

Experimental design

Pot experiments were conducted in a greenhouse at Zhejiang A&F University, China. Soil samples (0–20 cm depth) were collected from a Cd/As-contaminated paddy field in Jinhua City, Zhejiang Province, China. After being air-dried, homogenized, and sieved through a 2-mm sieve, 1.5 kg of soil was placed into plastic pots (10 cm in diameter, 12 cm in height). The amendments (BC, FH, FB, and SFB) were incorporated at rates of 1.0%, 2.0%, and 3.0% (w/w, dry weight), with untreated soil serving as the control. Each treatment was conducted in triplicate. During the 150-d incubation period, soil moisture was maintained at 60% of field capacity. After incubation, soils were air-dried, ground, and sieved (100 mesh) prior to analysis. Soil physicochemical properties are summarized in the Supplementary Material (S2.1 Soil properties).

Metal(liod)s availability and redistribution

Soil bioavailable Cd and As concentrations were determined using hydride generation-atomic fluorescence spectrometry (HG-AFS) and ICP-MS[27]. Sequential extraction was conducted following the BCR procedure to quantify acid-soluble (F1), reducible (F2), oxidizable (F3), and residual (F4) fractions[28]. Detailed methods are presented in the Supplementary Material (S1.4 Metal(liod)s redistribution).

Data quality control and statistical analysis

All experiments were conducted in triplicate, with relative standard deviations below 5%. Laboratory glassware was soaked in 3% HNO_3 for 24 h and rinsed thoroughly with deionized water prior to use. Statistical analyses were conducted using SPSS 26.0, with results expressed as mean ± standard error (n = 3). Significant differences were evaluated using one-way ANOVA ($p < 0.05$). Graphical outputs were generated using Origin 2021, and XPS spectra were analyzed using Thermo Avantage software.

Results and discussion

Characterization of the amendments

SEM-EDS analysis revealed distinct morphological and compositional differences among the synthesized amendments (Fig. 1). The BC exhibited a relatively smooth surface with well-developed macropores

https://doi.org/10.48130/aee-0026-0002

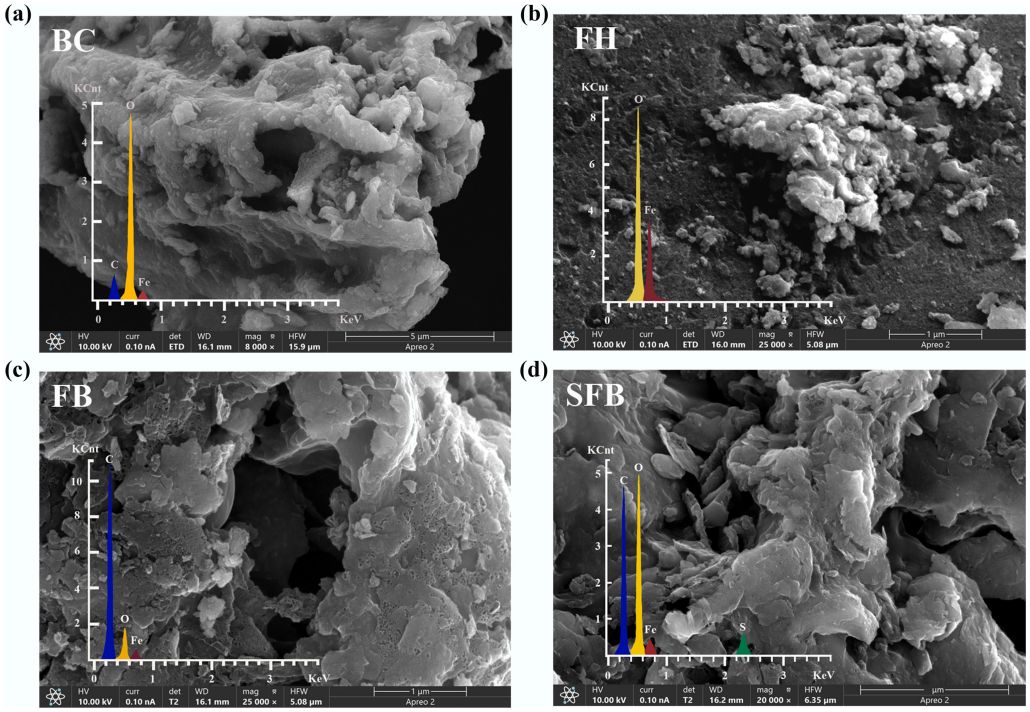

Fig. 1 SEM-EDS of amendments. (**a**) Biochar; (**b**) ferrihydrite, (**c**) ferrihydrite modified biochar; (**d**) sulfur-ferrihydrite modified biochar.

characteristic of lignocellulosic biochar, providing a structural framework for mineral loading. In contrast, FB displayed a markedly roughened surface with granular aggregates partially occluding the original pores (Table 1). The Fe content significantly ($p < 0.05$) increased from 4.41% in BC to 12.96% in FB, confirming the successful immobilization of ferrihydrite nanoparticles[29]. The homogeneous distribution of Fe distribution suggests the formation of stable Fe–O–C linkages between ferrihydrite hydroxyl groups and oxygen-containing functional groups on the biochar surface[30].

Sulfur modification induced further microstructural evolution. SFB exhibited a denser and more irregular morphology, with granular and flocculent coatings uniformly covering the biochar surface[31]. The emergence of a distinct sulfur signal (3.36%) in EDS spectra (Table 1) confirms effective sulfur incorporation and co-localization with Fe. This Fe–S co-enrichment indicates the formation of Fe–S microdomains or ferric sulfide-like clusters that function as multifunctional reactive sites for Cd and As immobilization via precipitation, surface complexation, and redox transformation[32].

The increased surface roughness and aggregation of SFB are attributed to sulfur-mediated interfacial bridging between Fe phases and carbon surfaces, enhancing particle cohesion and surface coverage[33]. Localized EDS mapping further supports the formation of a chemically integrated Fe–S–C matrix rather than a simple physical mixture[34,35]. This hierarchical architecture provides abundant reactive sites and redox-active centers, underpinning the superior stability and multifunctionality of SFB for Cd(II) and As(III) immobilization in complex systems[36].

Table 1 Characterization of amendments

Parameter	BC	FH	FB	SFB
Yield (% dry wt.)	50.12	N.D.	N.D.	N.D.
Ash (% dry wt.)	36.61	N.D.	N.D.	N.D.
pH	11.48	4.36	10.86	10.58
C (%)	10.58	0.00	61.43	36.72
O (%)	39.05	34.27	15.37	32.23
S (%)	0.00	0.00	0.00	3.36
Fe (%)	4.41	65.73	12.96	7.98
Surface area ($m^2\ g^{-1}$)	64.20	294.91	175.35	185.16
Pore volume ($cm^3\ g^{-1}$)	0.0696	0.1804	0.1263	0.1305
Pore diameter (nm)	4.84	2.46	3.05	2.89

N. D.: Not detected.

Removal performance of Cd(II) and As(III)

pH-dependence

The adsorption behaviors of Cd(II) and As(III) on BC, FH, FB, and SFB were strongly pH-dependent, reflecting the combined effects of metal speciation, surface charge evolution, and functional group availability. Cd(II) uptake increased sharply from pH 3.0 to 5.0, indicating reduced competition with protons for negatively charged surface sites (Fig. 2a). Above pH 5, adsorption either plateaued or slightly decreased, reaching equilibrium at approximately pH 7. Under acidic conditions, high H^+ concentrations induce electrostatic repulsion and reduce the availability of functional groups for Cd(II) binding, whereas at pH > 8, Cd predominantly precipitates as $Cd(OH)_2$, which accounts for the increased removal efficiency[37].

The adsorption of As(III) also exhibited pronounced pH dependence[38]. BC showed minimal responsiveness to pH, likely due to its limited surface functional groups (Fig. 2b), whereas FH, FB, and SFB displayed increasing adsorption from pH 3 to 8, followed by a sharp decline at higher pH. This behavior corresponds to As speciation: $H_2AsO_4^-$ dominates at pH 2–6, $HAsO_4^{2-}$ between pH 6–9, and AsO_4^{3-} at pH > 8. This trend reflects both arsenic speciation and surface charge evolution, with increasing electrostatic repulsion between negatively charged arsenate species and deprotonated surfaces at alkaline pH[30]. Notably, SFB maintained higher adsorption capacity across a broader pH range, attributable to sulfur induced surface-heterogeneity and increased site diversity[30,39].

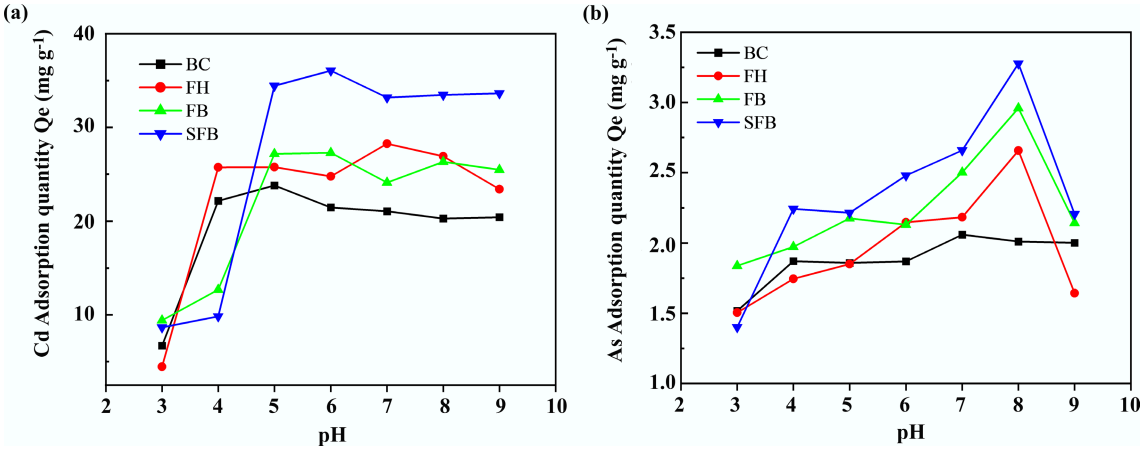

Fig. 2 Initial solution pH-dependent experiments of (**a**) Cd(II), and (**b**) As(III) adsorption on amendments. (BC: Biochar; FH: Ferrihydrite, FB: Ferrihydrite modified biochar; SFB: sulfur-ferrihydrite modified biochar).

Adsorption kinetics

As shown in Fig. 3, the adsorption kinetics of Cd(II) and As(III) exhibited time-dependent behavior characterized by rapid initial uptake followed by gradual equilibration. Cd(II) adsorption on FB occurred most rapidly, reaching equilibrium within approximately 60 min, whereas FH and BC required about 120 min (Fig. 3a). In contrast, SFB exhibited a longer equilibration time (approximately 480 min), reflecting a more complex adsorption process governed by chemisorption and intraparticle diffusion[40]. This extended equilibrium time is attributed to the progressive involvement of Fe–S reactive domains that facilitate strong surface complexation and potential redox interactions between Cd(II) and the Fe–S–C matrix[35]. For As(III), adsorption reached equilibrium within 60 min for all amendments (Fig. 3b), suggesting that its adsorption was dominated by rapid outer-sphere complexation and ligand exchange with ferric hydroxyl and carbon functional groups[41]. The markedly faster equilibration of As(III) compared to Cd(II) highlights the contrasting diffusion behavior and binding energetics of the two species, consistent with their differing ionic charges and coordination chemistries. The pseudo-second-order kinetic model fitted the experimental data with higher correlation coefficients (R^2 = 0.86–0.991 for Cd(II) and 0.931–0.979 for As(III) compared to the pseudo-first-order model (Table 2), indicating that chemisorption played the dominant role[42].

The multi-stage kinetic behavior of Cd(II) and As(III) adsorption by SFB follows the classical three-step pattern: (1) an initial fast phase dominated by electrostatic attraction and surface diffusion[14,16]; (2) a slower phase governed by chemical complexation with Fe–O and Fe–S functional groups[20]; and (3) an equilibrium phase characterized by gradual saturation of surface sites[36]. Among all amendments, the SFB composite exhibited the highest equilibrium adsorption capacity, reaching 26.42 mg g^{-1} for Cd(II), and 4.08 mg g^{-1} for As(III) (Table 2). This superior performance can be attributed to the co-presence of Fe-S reactive clusters and carbon functional domains that facilitate both inner-sphere coordination with Cd(II) and redox-mediated transformation of As(III) to As(V)[43]. The slower equilibrium of SFB relative to BC further supports that its adsorption involves multi-step surface reactions, including ion exchange, complexation, and redox coupling at Fe–S–C interfaces, rather than simple diffusion-limited adsorption[34].

Adsorption isotherms

The equilibrium adsorption isotherms provide further insight into the interaction mechanisms governing Cd(II) and As(III) immobilization (Fig. 4). The adsorption capacities of all amendments increased with rising initial concentrations of the metal(loid)s and subsequently

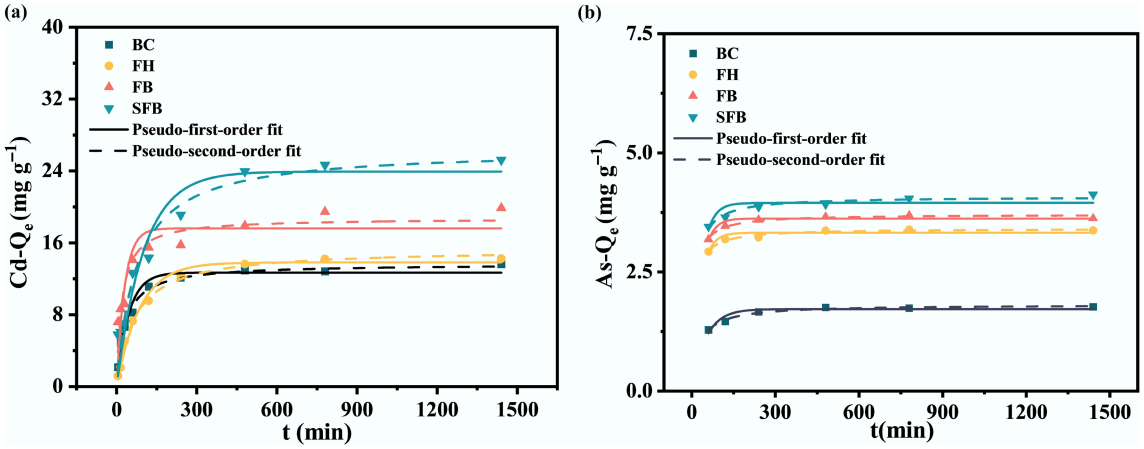

Fig. 3 Kinetic of (**a**) Cd(II), and (**b**) As(III) adsorption on amendments. (BC: Biochar; FH: Ferrihydrite, FB: Ferrihydrite modified biochar; SFB: sulfur-ferrihydrite modified biochar).

https://doi.org/10.48130/aee-0026-0002

Table 2 Kinetic parameters for Cd(II) and As(III) adsorption onto amendments

Toxic metal(loid)s	Amendments	Pseudo first-order model			Pseudo second-order model		
		R^2	K_1	Q_e (mg g^{-1})	R^2	K_2	Q_e (mg g^{-1})
Cd	BC	0.955	0.002	12.68	0.991	0.002	13.65
	FH	0.986	0.001	13.81	0.995	0.001	15.32
	FB	0.730	0.003	17.60	0.860	0.003	18.73
	SFB	0.896	0.001	23.93	0.941	0.01	26.42
As	BC	0.845	0.021	1.72 ± 0.04	0.979	0.022	1.81 ± 0.02
	FH	0.974	0.035	3.32 ± 0.04	0.961	0.030	3.42 ± 0.02
	FB	0890	0.034	3.62 ± 0.03	0.956	0.028	3.71 ± 0.02
	SFB	0.926	0.056	3.95 ± 0.08	0.931	0.022	4.08 ± 0.04

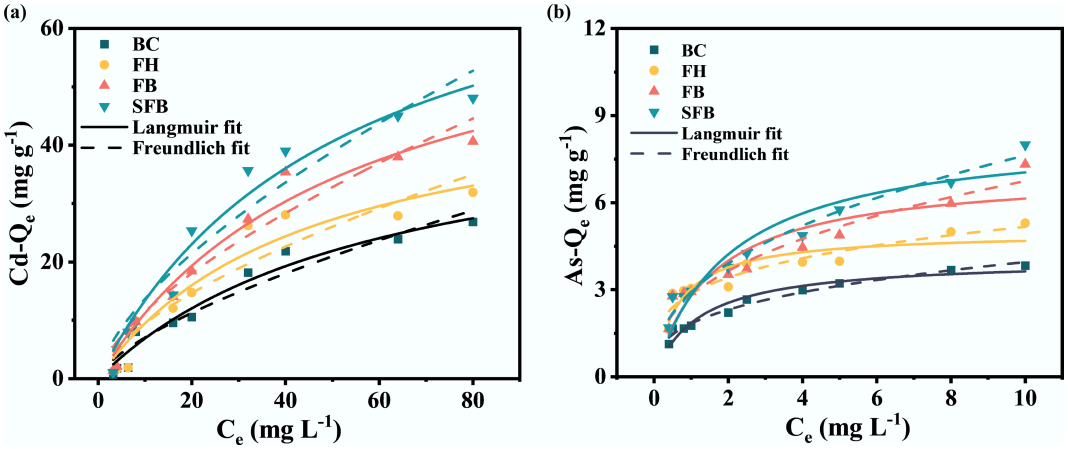

Fig. 4 Isotherms of (**a**) Cd(II), and (**b**) As(III) adsorption on amendments. (BC: Biochar; FH: Ferrihydrite, FB: Ferrihydrite modified biochar; SFB: sulfur-ferrihydrite modified biochar).

approached saturation, consistent with the occupation of a finite number of reactive sites.

For Cd(II), the Langmuir model yielded higher correlation coefficients (R^2 = 0.905–0.959) than the Freundlich model (R^2 = 0.835–0.917), implying that monolayer adsorption predominates on relatively homogeneous active surfaces (Table 3, Fig. 4a). The maximum adsorption capacity (Q_m) followed the order SFB (76.69 mg g^{-1}) > FB (64.44 mg g^{-1}) > FH (45.28 mg g^{-1}) > BC (41.36 mg g^{-1}), highlighting the enhancement in adsorption potential resulting from ferrihydrite and sulfur co-modification. This enhancement is closely linked to the formation of Fe–O–C and Fe–S–C linkages that provide high-energy binding domains for Cd(II) complexation and precipitation[44,45].

For As(III), the Freundlich model provided a better fitting of the adsorption data (R^2 = 0.886–0.979), indicating that multilayer adsorption occurred on heterogeneous surfaces containing diverse reactive sites (Table 3, Fig. 4b). The Freundlich constant 1/n > 1 for all amendments, particularly for SFB (1/n = 2.94), demonstrates favorable adsorption conditions and strong affinity toward As(III). The SFB composite achieved a maximum adsorption capacity of 8.28 mg g^{-1}. The superior As(III) retention can be attributed to redox-active Fe–S microdomains that facilitate the oxidation of As(III) to As(V), followed by strong inner-sphere complexation with Fe(III) hydroxyl groups[45]. This redox-complexation coupling mechanism explains the distinctly higher adsorption performance of SFB relative to other amendments and demonstrates the cooperative functionality of the Fe and S components within the carbon matrix[26]. Therefore, these results reveal that the dual modification (iron and sulfur) of biochar produces a synergistic adsorption system capable of concurrently capturing both cationic and anionic species through complementary mechanisms.

Cd(II) and As(III) removal mechanisms

The FTIR spectra (Fig. 5a) provided molecular-level evidence for the evolution of surface functional groups following ferrihydrite and sulfur modification, as well as after Cd(II) and As(III) adsorption. BC exhibited characteristic absorption bands at 1,590.30 and 1,020.15 cm^{-1}, attributable to C=O stretching and C–O–C vibrations, respectively[41]. In FB, the broad –OH stretching band intensified and shifted from 3,364 to 3,371 cm^{-1}, indicating an increased abundance of surface hydroxyl groups and enhanced hydrogen-bonding capacity[14]. Concurrently, new bands at 1,624 and 576 cm^{-1} appeared, corresponding to Fe–OH bending and Fe–O lattice vibrations, respectively, confirming the successful deposition of Fe oxyhydroxide phases on the biochar surface[24,35]. Subsequent sulfur modification induced additional spectral features at approximately 1,632 and 1,112 cm^{-1}, corresponding to C=O/C=C and C–S stretching vibrations, respectively, indicating the effective incorporation of sulfur-containing functionalities. After Cd(II) and As(III) adsorption, the Fe–O vibration shifted from 576 to 570 cm^{-1}, while the –OH stretching band broadened and shifted toward higher wavenumbers (3,363.96 to 3,371.64 cm^{-1}), indicating the transformation of surface hydroxyl and Fe–O groups into Fe–O–Cd and Fe–O–As coordination structures[46,47]. The appearance of new peaks (C=O) around 1,630–1,640 cm^{-1} further suggests partial oxidation of As(III) to As(V), likely mediated by interfacial electron transfer involving Fe(III) species within the ferrihydrite domain[48]. Overall, these FTIR results demonstrate that oxygen- and sulfur-containing functional groups, including –OH, C=O, and C–S,

Table 3 Isotherms parameters for Cd(II) and As(III) adsorption onto amendments

Toxic metal(loid)s	Amendments	Langmuir parameters			Freundlich parameters		
		R^2	b	Q_m (mg g^{-1})	R^2	K_f	1/n
Cd	BC	0.936	0.021	41.36	0.899	0.637	1.68
	FH	0.905	0.027	45.28	0.835	0.591	2.48
	FB	0.960	0.022	64.44	0.917	0.628	2.75
	SFB	0.959	0.022	76.69	0.914	0630	3.24
As	BC	0.939	0.841	4.06	0.976	0.333	1.84
	FH	0.798	1.552	4.98	0.886	0.256	2.86
	FB	0.846	0.846	6.72	0.961	0.361	2.84
	SFB	0.902	0.522	8.28	0.979	0.409	2.94

jointly participate in Cd and As immobilization through inner-sphere complexation, hydrogen bonding, and redox-assisted coordination, leading to the formation of an integrated Fe–S–C interfacial structure[44]. Compared with previously reported Fe-modified biochars, which primarily rely on Fe–O complexation and exhibit limited Cd precipitation capacity, or S-modified biochars, which favor CdS formation but poorly retain anionic arsenic species, the co-existence of Fe and S in SFB generates unified Fe–S reactive microdomains that simultaneously enable Fe–O–As bonding and sulfide-mediated Cd(II) precipitation. This integrated functionality represents a defining structural advantage of SFB over single-modified or amendment material systems.

The SEM-EDS mapping (Fig. 5b) results further provide direct microstructural evidence supporting the distinct immobilization mechanisms of Cd(II) and As(III). BC exhibited a porous and relatively rough surface (Fig. 5b[I]), facilitating physical adsorption but resulting in limited Cd(II) (1.38%) and As(III) (1.40%) uptake. FH displayed aggregated fine particles (Fig. 5b[II]) and showed a stronger affinity for Ass(III) (4.28%) than for Cd(II) (1.31%) adsorption, reflecting the inherent preference of ferrihydrite for arsenic oxyanions via oxidative complexation[49]. In contrast, FB exhibits a denser and smoother morphology (Fig. 5b[III]), accompanied by lower Cd(II) (0.43%) and As(III) (0.74%) contents, suggesting a reduced availability of accessible reactive sites[16]. Notably, SFB exhibited a coarse, flaky surface morphology with a homogeneous and co-localized distribution of Cd(II) (1.89%), and As(III) (2.76%) (Fig. 5b[IV]). This spatial co-localization confirms that sulfur modification effectively integrates the high As(III) affinity of ferrihydrite with the porous biochar framework, generating synergistic interfacial domains conducive to concurrent immobilization of both contaminants[22,30]. The pronounced Cd signals indicate sequestration via ion exchange and surface complexation, whereas the strong As signals reflect As(III) oxidation followed by precipitation and/or complexation with iron oxides[50]. These direct visual observations corroborate the adsorption model, confirming that the superior immobilization efficiency of SFB derives from a cooperative mechanism involving both physical adsorption and chemisorption, effectively transforming Cd(II) and As(III) into more stable and environmentally inert forms. This morphological evidence further explains why SFB outperforms previously reported Fe-only or S-only modified biochars. The adsorption capacities obtained in this work (Cd: 76.69 mg g^{-1}; As: 8.28 mg g^{-1}) exceed those commonly reported for single-modified systems, demonstrating that neither Fe-only nor S-only materials generate structures capable of such co-localized immobilization of both Cd and As. The coarse, flaky microstructure of SFB thus reflects not only sulfur incorporation but also the cooperative Fe–S interactions that create multifunctional interfacial sites suitable for dual-contaminant capture.

XPS analysis (Fig. 6) further elucidates the surface electronic structure and bonding mechanisms responsible for Cd(II) and As(III) retention by SFB. After adsorption, distinct Cd 3d (405–412 eV) and As 3d (1,326–1,362 eV) signals were detected, confirming successful

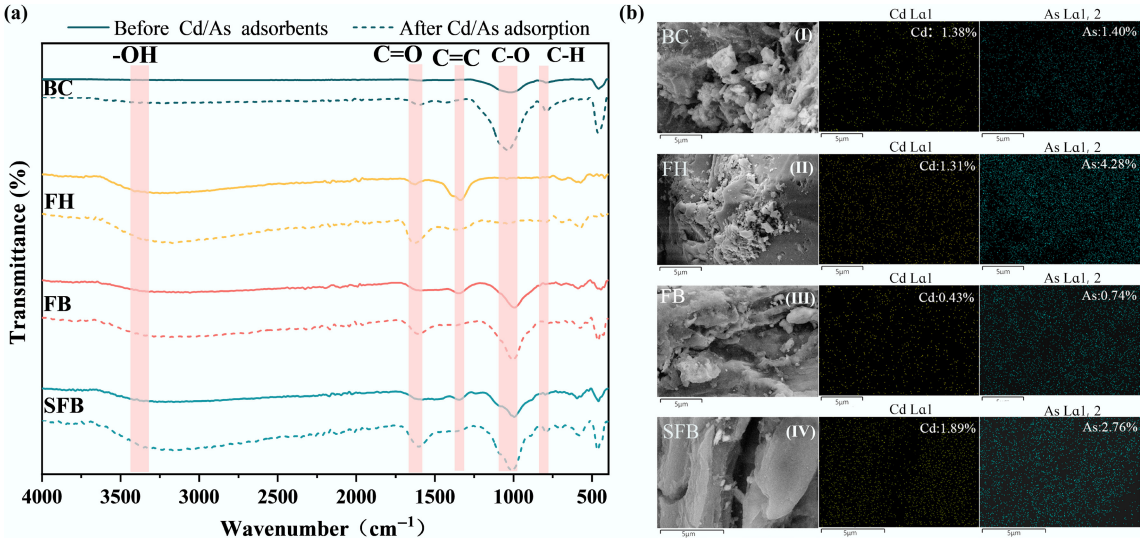

Fig. 5 (**a**) FTIR, and (**b**) SEM-mapping spectra of amendments before and after Cd(II) and As(III) sorption. (BC: Biochar; FH: Ferrihydrite, FB: Ferrihydrite modified biochar; SFB: sulfur-ferrihydrite modified biochar).

https://doi.org/10.48130/aee-0026-0002

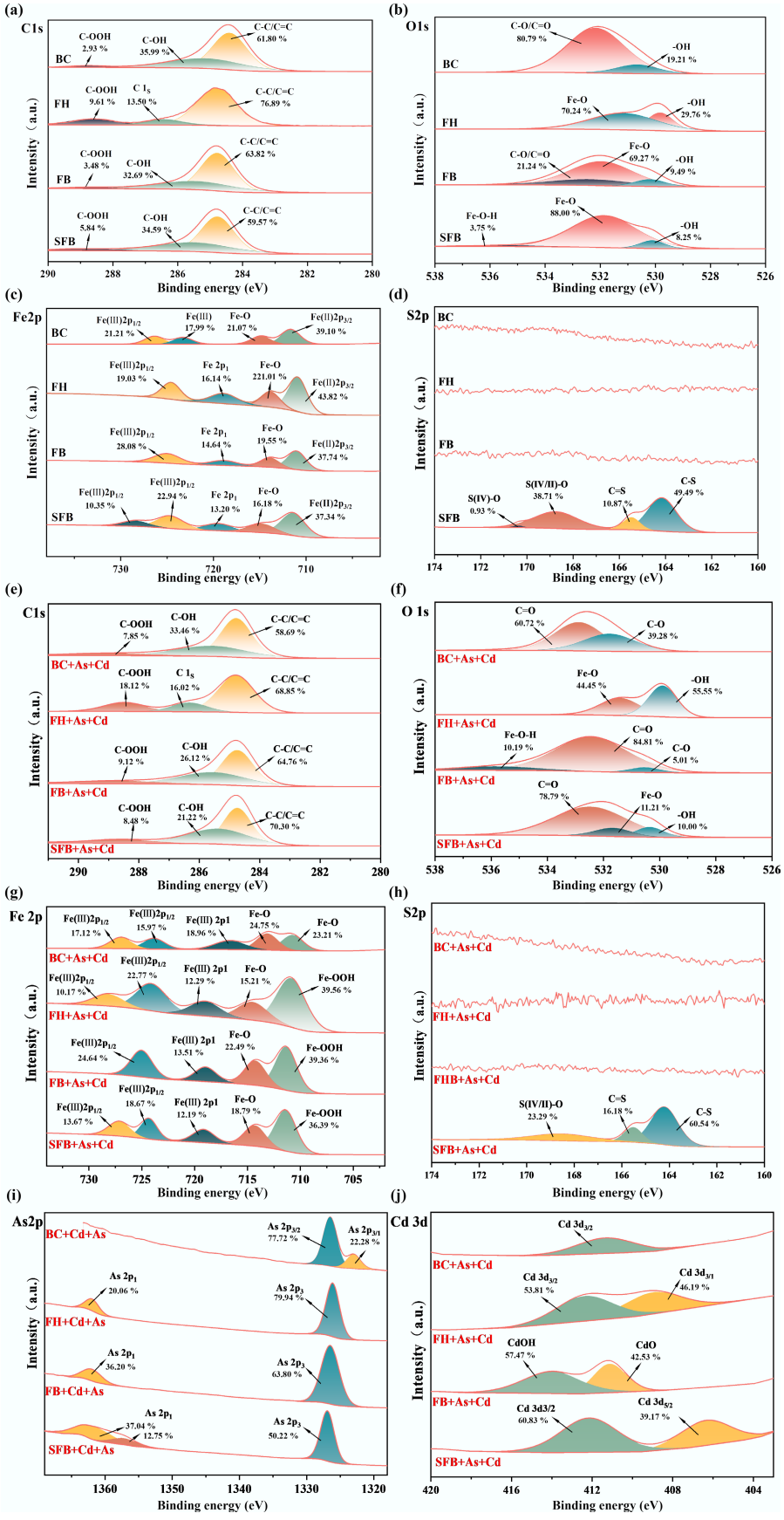

Fig. 6 XPS spectra of C 1s, O 1s, Fe 2p, S 2p for amendments (**a**)–(**d**) before, and (**e**)–(**h**) after Cd(II) and As(III) adsorption; and (**i**) As 2p, and (**j**) Cd 3d for amendments after Cd(II) and As(III) adsorption. (BC: Biochar; FH: Ferrihydrite, FB: Ferrihydrite modified biochar; SFB: sulfur-ferrihydrite modified biochar).

contaminant capture. Deconvolution of the C 1s spectra revealed three principal components at 284.6 eV (C–C/C=C), 285.8 eV (C–OH), and 288.4 eV (C=O/C–OOH), with a decline in intensities of C–OH and C=O after adsorption (Fig. 6a, e), indicating their involvement in metal(loids) coordination[14]. The O 1s spectra displayed a reduction in Fe-OH (531.1 eV) and a concomitant increase in Fe–O (530.1 eV), consistent with the formation of Fe–O–Cd/As inner-sphere complexes[35] (Fig. 6b, f). A weak shoulder at 535.3 eV further supports Fe–O–As(V) complex formation via ligand exchange[45]. The Fe 2p spectra revealed the coexistence of Fe(II) and Fe(III) species, with a positive shift (0.4 eV) in Fe $2p_{3/2}$ binding energy after adsorption, indicating partial Fe(III) reduction coupled with As(III) oxidation (Fig. 6c, g). This redox coupling enhances Fe-S surface reactivity and stabilizes both metal species[23]. The S 2p spectra exhibited characteristic peaks at 164.2, 165.5, and 168.8 eV, attributed to C–S, C=S, and S–O bonds[51,52] (Fig. 6d, h). The relative proportion of oxidized sulfur (S–O) decreased from 39.6% to 23.3% after adsorption, confirming sulfur participation in reduction reactions and the formation of CdS precipitates[53]. Interestingly, the new peaks at 1,326, 1,362, 412, and 405 eV in As(III)/Cd(II)-laden amendments, as presented in Fig. 6i and j, were due to electrons from the As 2p and Cd 3d levels, respectively, indicating that As(III) and Cd(II) were captured by the SFB. Importantly, the XRD peaks confirm the formation of FeS phases (Supplementary Material, S2.2 Structural characterization of the amendments). These electronic-structure characteristics confirm that Cd(II) sequestration proceeds through ion exchange, inner-sphere complexation, and CdS/FeS precipitation, while As(III) is oxidized to As(V) and subsequently forms Fe–O–As complexes. Such simultaneous processes, sulfide precipitation for Cd(II) and oxidative complexation for As(III), are rarely attainable in single-modified biochars and provide strong evidence for the synergistic effect arising from Fe–S dual modification.

In summary, Cd(II) and As(III) immobilization by SFB involves multiple coupled mechanisms as shown in Fig. 7[54,55]: (1) inner-sphere complexation involving Fe–O, C–O, and C-S functional groups; (2) precipitation and co-precipitation of CdS and Fe–S mineral phases; and (3) redox-mediated oxidation of As(III) concomitant with Fe(III)/Fe(II) and S(II)/S(IV) transformations. This cooperative Fe-S interaction enables effective stabilization of both cationic and anionic contaminants, providing a level of multifunctionality unattainable by conventional Fe-only or S-only biochars.

Effects of amendments on As(III) and Cd(II) availability and fraction in soil

Application of all amendments significantly reduced the concentrations of dissolved Cd(II) and As(III) (except FH treatments) in soil over the incubation period (Supplementary Material, S2.3 Effect of amendments on soil Cd/As availability). Among all treatments, the SFB treatments resulted in a decline in $CaCl_2$-extractable Cd(II) (Fig. 8a). Compared to the control, all SFB treatments exhibited statistically significant ($p < 0.05$) reductions, with Cd(II) concentrations declining from 0.15 to 0.06–0.07 mg kg^{-1}, corresponding to reductions of 32.59% to 41.26%. The lowest concentration of the $CaCl_2$-extractable Cd(II) was observed in the 3% SFB treatment. Similarly, the NaH_2PO_4-extractable As(III) concentration in soil decreased following SFB addition (Fig. 8b). Relative to the control (2.40 mg kg^{-1}), As(III) levels declined to 0.86–1.20 mg kg^{-1} across the SFB treatments, representing a significant ($p < 0.05$) reduction of 50.06%–64.06%. The 3% SFB treatment also achieved the greatest reduction.

SFB addition also significantly altered the distribution of fractions of Cd(II) and As(III) in soil (Fig. 8c, d). In the 3% SFB treatment, the proportions of labile Cd(II) fractions (F1, F2, and F3) decreased by 60.64%, 20.50%, and 37.24%, respectively, whereas the F4 fraction increased by 87.89% in soil relative to the control. A similar trend was observed for soil As(III), with F1, F2, and F3 fractions declining by 7.5%–45.9% and a corresponding increase of 33.6%–41.9% in the F4 fraction. This fraction redistribution indicates a pronounced shift from readily bio-available forms toward more stable and immobilized species, highlighting the effectiveness of SFB in reducing metal mobility and enhancing soil chemical stability[36,40].

Conclusions

The sulfur-ferrihydrite-modified biochar (SFB) synthesized in this study

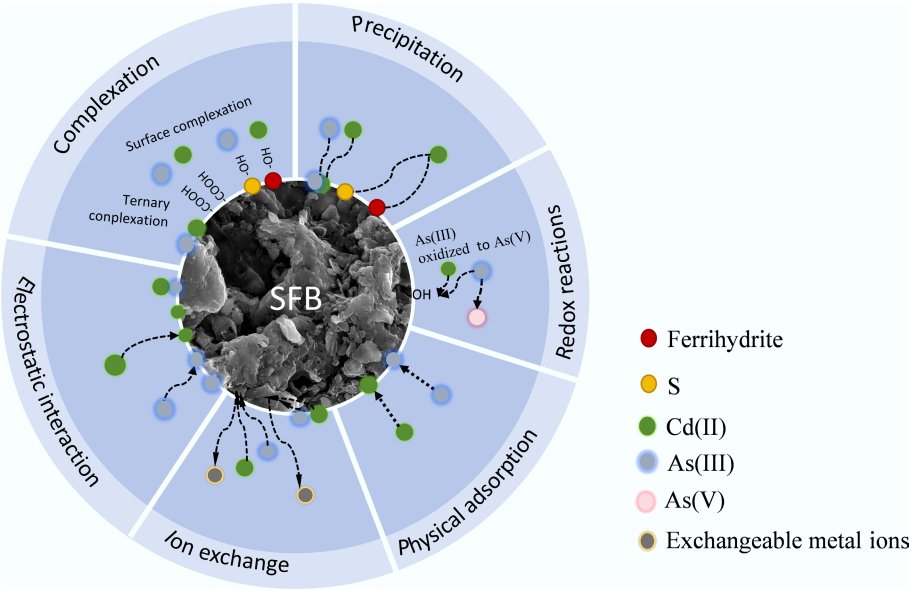

Fig. 7 The potential mechanisms of Cd (II) and As(III) by SFB.

https://doi.org/10.48130/aee-0026-0002

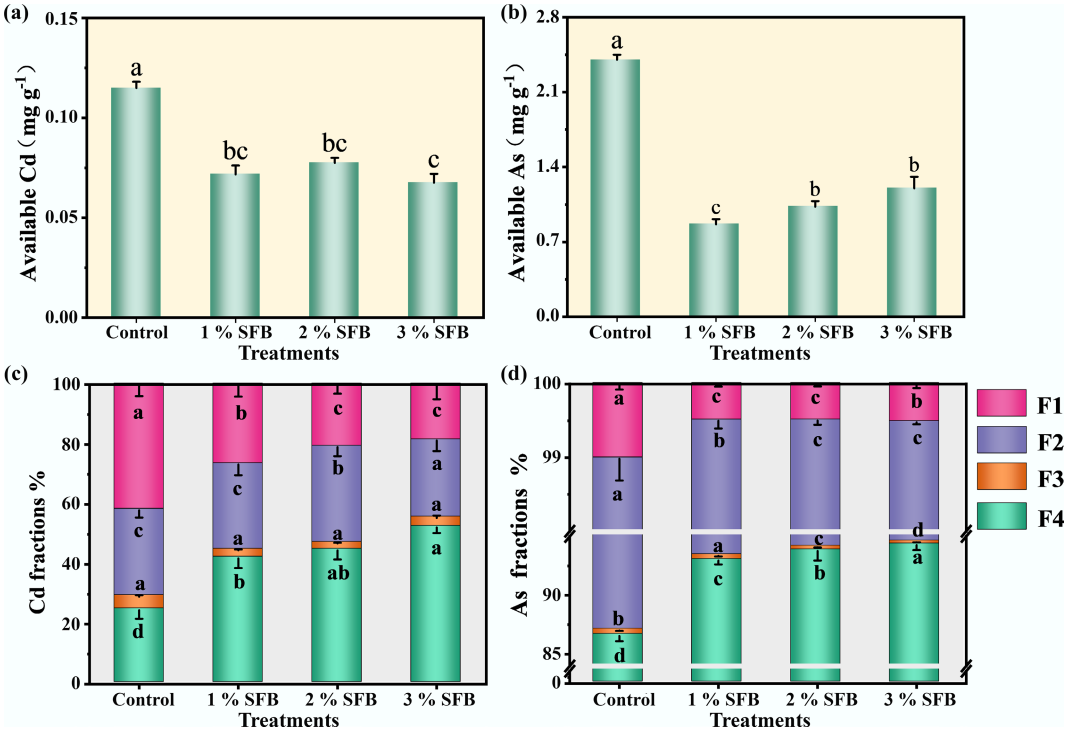

Fig. 8 The available and fraction of (**a**), (**c**) Cd(II), and (**b**), (**d**) As(III) in soil after amended by SFB. F1: the acid soluble fraction; F2: the reducible fraction; F3: the oxidizable fraction; F4: the residual fraction. Data points and error bars represent mean ± S.D. (n = 3). Different letters indicate a significant difference (p < 0.05). (BC: Biochar; FH: Ferrihydrite, FB: Ferrihydrite modified biochar; SFB: sulfur-ferrihydrite modified biochar).

effectively immobilized Cd(II) and As(III) in both aqueous and soil environments. Its enhanced adsorption capacity and robust performance in Cd(II)/As(III) systems, across a wide pH spectrum, can be attributed to its increased surface area, hierarchical porosity, and abundant oxygen- and sulfur-containing functional groups relative to the pristine biochar. The removal of Cd and As(III) was governed by multiple synergistic mechanisms, including electrostatic attraction, ion exchange, precipitation, and the formation of stable inner- and outer-sphere complexes, and facilitated concurrent immobilization. Notably, the presence of As(III) enhanced Cd(II) adsorption, likely due to As(III)-induced modifications of surface charge and improved dispersion of biochar on ferrihydrite, reflecting the complex interplay between cationic and anionic species in multi-metal systems. Application of SFB to contaminated soils substantially reduced bioavailable Cd(II) and As(III) concentrations by 34.98% and 78.27%, respectively, and promoted their transformation into more stable residual fractions. Overall, SFB shows significant promise as a multifunctional amendment for the remediation of Cd(II) and As(III) contaminated environments, offering strong adsorption capacity, structural stability, and mechanistic versatility, with implications for long-term remediation applications. Future studies will quantitatively determine sulfur speciation and redox pathways (such as SO_4^{2-} production, reduced sulfur species, and potential H_2S volatilization), monitor soil pH evolution, acid-neutralizing capacity, and buffering responses during sulfur oxidation, conduct extended leaching and ageing experiments under a range of redox and moisture conditions to evaluate long-term stability, and assess H_2S generation risks under anaerobic or flooded conditions.

Supplementary information

It accompanies this paper at: https://doi.org/10.48130/aee-0026-0002.

Author contributions

The authors confirm their contributions to the paper as follows: Weijie Xu: conceptualization, formal analysis, writing – original draft; Dong Huang: formal analysis, visualization; Houbo Huang: formal analysis, visualization; Xiaowen Teng: data curation, software; Ijlal Ahmad: data curation, software, writing – review & editing; Bo Zheng: writing – review & editing; Hanbo Chen: writing – review & editing; Yaqian Li: conceptualization; Dan Liu: funding acquisition, project administration. All authors reviewed the results and approved the final version of the manuscript.

Data availability

The datasets used or analyzed during the current study are available from the corresponding author upon reasonable requests.

Funding

This study was funded by the Natural Science Foundation of China (Grant Nos 32271532, 42407016), Zhejiang Provincial Natural Science Foundation of China (Grant No. MS26D010008), and Research and Development Fund of Zhejiang A&F University (Grant No. 2020LFR052).

Declarations

Competing interests

The authors declare that they have no conflict of interest.

Author details

[1]Zhejiang Key Laboratory of Soil Remediation and Quality Improvement, College of Environment and Resources, College of Carbon Neutrality, Zhejiang A&F University, Hangzhou 311300, China; [2]Pujiang County Ecological Civilization Promotion Center, Jinhua 322200, China; [3]Department of Livestock Management, Breading and Genetics, The University of Agriculture, Peshawar 25000, Pakistan; [4]School of Environment and Natural Resources, Zhejiang University of Science & Technology, Hangzhou 310023, China; [5]People's Government of Yanguan Town, Jiaxing 314000, China

References

[1] Lyu P, Li L, Huang X, Wang G, Zhu C. 2022. Pre-magnetic bamboo biochar cross-linked Ca–Mg–Al layered double-hydroxide composite: high-efficiency removal of As(III) and Cd(II) from aqueous solutions and insight into the mechanism of simultaneous purification. *Science of The Total Environment* 823:153743

[2] Zhou S, Liu Z, Sun G, Zhang Q, Cao M, et al. 2022. Simultaneous reduction in cadmium and arsenic accumulation in rice (*Oryza sativa* L.) by iron/iron-manganese modified sepiolite. *Science of The Total Environment* 810:152189

[3] Adnan M, Xiao B, Xiao P, Zhao P, Li R, et al. 2022. Research progress on heavy metals pollution in the soil of smelting sites in China. *Toxics* 10(5):231

[4] Gong Y, Qu Y, Yang S, Tao S, Shi T, et al. 2020. Status of arsenic accumulation in agricultural soils across China (1985–2016). *Environmental Research* 186:109525

[5] Sun S, Huang J, Wen J, Peng Z, Zhang N, et al. 2024. Sepiolite-supported nanoscale zero-valent iron alleviates Cd&As accumulation in rice by reducing Cd&As bioavailability in paddy soil and promoting Cd&As sequestration in iron plaque. *Environmental Technology & Innovation* 33:103540

[6] Qiao JT, Liu TX, Wang XQ, Li FB, Lv YH, et al. 2018. Simultaneous alleviation of cadmium and arsenic accumulation in rice by applying zero-valent iron and biochar to contaminated paddy soils. *Chemosphere* 195:260–271

[7] Shen B, Wang X, Zhang Y, Zhang M, Wang K, et al. 2020. The optimum pH and Eh for simultaneously minimizing bioavailable cadmium and arsenic contents in soils under the organic fertilizer application. *Science of The Total Environment* 711:135229

[8] Huang BY, Zhao FJ, Wang P. 2022. The relative contributions of root uptake and remobilization to the loading of Cd and As into rice grains: implications in simultaneously controlling grain Cd and As accumulation using a segmented water management strategy. *Environmental Pollution* 293:118497

[9] Vaňková Z, Vítková M, Trakal L, Seyedsadr S, Miller OA, et al. 2021. Soil moisture influences performance of selected stabilizing amendments in soil remediation. *Geoderma* 402:115307

[10] Zou R, Qian M, Wang C, Mateo W, Wang Y, et al. 2022. Biochar: from by-products of agro-industrial lignocellulosic waste to tailored carbon-based catalysts for biomass thermochemical conversions. *Chemical Engineering Journal* 441:135972

[11] Yang X, Li J, Liang T, Yan X, Zhong L, et al. 2021. A combined management scheme to simultaneously mitigate As and Cd concentrations in rice cultivated in contaminated paddy soil. *Journal of Hazardous Materials* 416:125837

[12] Zhi M, Liu S, Hong Z, Wu N. 2014. Electrospun activated carbon nanofibers for supercapacitor electrodes. *RSC Advances* 4(82):43619–43623

[13] Tan XF, Liu SB, Liu YG, Gu YL, Zeng GM, et al. 2017. Biochar as potential sustainable precursors for activated carbon production: Multiple applications in environmental protection and energy storage. *Bioresource Technology* 227:359–372

[14] Zeng W, Lu Y, Zhou J, Zhang J, Duan Y, et al. 2024. Simultaneous removal of Cd(II) and As(V) by ferrihydrite-biochar composite: enhanced effects of As(V) on Cd(II) adsorption. *Journal of Environmental Sciences* 139:267–280

[15] Palansooriya KN, Shaheen SM, Chen SS, Tsang DCW, Hashimoto Y, et al. 2020. Soil amendments for immobilization of potentially toxic elements in contaminated soils: a critical review. *Environment International* 134:105046

[16] Hong C, Dong Z, Zhang J, Zhu L, Che L, et al. 2022. Effectiveness and mechanism for the simultaneous adsorption of Pb(II), Cd(II) and As(III) by animal-derived biochar/ferrihydrite composite. *Chemosphere* 293:133583

[17] Cui H, Bao B, Cao Y, Zhang S, Shi J, et al. 2022. Combined application of ferrihydrite and hydroxyapatite to immobilize soil copper, cadmium, and phosphate under flooding-drainage alternations. *Environmental Pollution* 292:118323

[18] Liu C, Yu HY, Liu C, Li F, Xu X, et al. 2015. Arsenic availability in rice from a mining area: is amorphous iron oxide-bound arsenic a source or sink? *Environmental Pollution* 199:95–101

[19] Qu J, Yuan Y, Zhang X, Wang L, Tao Y, et al. 2022. Stabilization of lead and cadmium in soil by sulfur-iron functionalized biochar: performance, mechanisms and microbial community evolution. *Journal of Hazardous Materials* 425:127876

[20] Du H, Nie N, Rao W, Lu L, Lei M, et al. 2021. Ferrihydrite–organo composites are a suitable analog for predicting Cd(II)–As(V) coexistence behaviors at the soil solid-liquid interfaces. *Environmental Pollution* 290:118040

[21] Bai Z, Fan X, Meng F, Zhao Y, Song B, et al. 2022. Study on high-efficiency arsenic removal performance and mechanism of carbon-supported ferrihydrite adsorbent. *Journal of Ecology and Rural Environment* 38(3):358–366 (in Chinese)

[22] Tian L, Liang Y, Lu Y, Peng L, Wu P, et al. 2018. Pb(II) and Cu(II) adsorption and desorption kinetics on ferrihydrite with different morphologies. *Soil Science Society of America Journal* 82(1):96–105

[23] Wu C, Shi L, Xue S, Li W, Jiang X, et al. 2019. Effect of sulfur-iron modified biochar on the available cadmium and bacterial community structure in contaminated soils. *Science of The Total Environment* 647:1158–1168

[24] Rajendran M, Shi L, Wu C, Li W, An W, et al. 2019. Effect of sulfur and sulfur-iron modified biochar on cadmium availability and transfer in the soil–rice system. *Chemosphere* 222:314–322

[25] Yin Z, Liu N, Bian S, Li J, Xu S, et al. 2019. Enhancing the adsorption capability of areca leaf biochar for methylene blue by K_2FeO_4-catalyzed oxidative pyrolysis at low temperature. *RSC Advances* 9(72):42343–42350

[26] Qiao Y, Hou D, Lin Z, Wei S, Chen J, et al. 2023. Sulfur fertilization and water management ensure phytoremediation coupled with Argo-production by mediating rhizosphere microbiota in the *Oryza sativa* L.-*Sedum alfredii* Hance rotation system. *Journal of Hazardous Materials* 457:131686

[27] Yang X, Dai Z, Ge C, Yu H, Bolan N, et al. 2023. Multiple-functionalized biochar affects rice yield and quality via regulating arsenic and lead redistribution and bacterial community structure in soils under different hydrological conditions. *Journal of Hazardous Materials* 443:130308

[28] Ure AM, Quevauviller P, Muntau H, Griepink B. 1993. Speciation of heavy metals in soils and sediments: an account of the improvement and harmonization of extraction techniques undertaken under the auspices of the BCR of the commission of the European communities. *International Journal of Environmental Analytical Chemistry* 51:135–151

[29] Song Z, Liao R, Su X, Zhang X, Zhao Z, et al. 2023. Development of a novel three-dimensional biofilm-electrode system (3D-BES) loaded with Fe-modified biochars for enhanced pollutants removal in landfill leachate. *Science of The Total Environment* 903:166980

[30] Jiang M, Wang K, Li G, Zhao Q, Wang W, et al. 2023. Stabilization of arsenic, antimony, and lead in contaminated soil with montmorillonite modified by ferrihydrite: efficiency and mechanism. *Chemical Engineering Journal* 457:141182

[31] Liu Q, Chen Z, Chen Z, Pan X, Luo J, et al. 2023. Microbial community

characteristics of cadmium speciation transformation in soil after iron-based materials application. *Applied Soil Ecology* 183:104745
[32] Li Q, Ma X, Qi C, Li R, Zhang W, et al. 2022. Facile preparation of novel magnetic mesoporous Fe-Mn binary oxides from mn encapsulated carboxymethyl cellulose-Fe(III) hydrogel for antimony removal from water. *Science of The Total Environment* 821:153529
[33] Yang J, Shi X, Sun Z. 2025. Polyethylene glycol-enhanced CoFe alloy @biochar to boost Fenton-like reactions: a synergy of $SO_4^{\cdot-}$, $^1O_2$, Co(IV)/Fe(IV) and electron transfer. *Environmental Research* 285(4):122593
[34] Yang S, Deng H, Mehta N, Zhu X, Wang H, et al. 2025. Pyrolysis temperature dependent electron mediating mechanisms of biochar for microbial reduction of Fe(III)-rich smectite. *Applied Clay Science* 276:107960
[35] Li P, Lu H, Yang J, Li Q, Liu F, et al. 2025. Persulfate activation by sulfur-doped zero-valent iron @biochar for nitroaromatics removal: Coexisting oxidation and reduction processes. *Journal of Water Process Engineering* 79:108893
[36] Zheng X, Wu Q, Huang C, Wang P, Cheng H, et al. 2023. Synergistic effect and mechanism of Cd(II) and As (III) adsorption by biochar supported sulfide nanoscale zero-valent iron. *Environmental Research* 231:116080
[37] Chen X, Si T, Wang S, Yuan R, Bian R, et al. 2025. Enhancement of soil DOC and electron transport by biochar strengthens Cd immobilization via iron oxides transformations in waterlogged soils. *Journal of Environmental Management* 391:126532
[38] Yang X, Yang F, Liu C, Sun H, Hou D, et al. 2025. Adsorption characteristics and mechanism insights of K_2FeO_4 coupling with $ZnCl_2$-assisted modified functionalized biochar for Pb (II) in wastewater. *Journal of Environmental Chemical Engineering* 13(1):115279
[39] Huang T, Imran I. 2025. Mitigating cadmium contamination in soil using Biochar, sulfur-modified Biochar, and other organic amendments. *International Journal of Phytoremediation* 27(6):874–887
[40] Ali Ahmad I, Hu H, Islam MS, Fu Q, Zhu J, et al. 2025. Simultaneous adsorption of cadmium and arsenic by goethite-modified rice straw-derived biochar in water and soil: interactive ion effects and co-adsorption mechanism. *Environmental Monitoring And Assessment* 197(6):648
[41] Wang M, Lai Y, Wang X, Zhang M, Han W, et al. 2025. Molecular insights into the simultaneous removal mechanisms of As(V) and Cd(II) in iron tailings slag-biochar composites. *Journal of Environmental Sciences* 154:470–482
[42] Giri PM, Parathasarathy P. 2025. Adsorption study on hexavalent chromium removal using magnetic biochar from *Ziziphus jujube* seed. *Chemical Engineering & Technology* 48:e70003
[43] Lin L, Zhang G, Liu X, Khan ZH, Qiu W, et al. 2019. Synthesis and adsorption of Fe-Mn-La-impregnated biochar composite as an adsorbent for As(III) removal from aqueous solutions. *Environmental Pollution* 247:128–135
[44] Yang F, Zhao L, Gao B, Xu X, Cao X. 2016. The interfacial behavior between biochar and soil minerals and its effect on biochar stability. *Environmental Science & Technology* 50(5):2264–2271
[45] Wang J, Huang J, Meng J, Pan G, Li Y, et al. 2025. Green synthesized nanoscale zero-valent iron impregnated tea residue biochar efficiently captures metal(loid)s for sustainable water remediation. *Journal of Environmental Management* 373:123585
[46] Li X, Chen H, Rong K, Gao Q, Jin J, et al. 2025. Removal of aqueous As(V) by biochar stabilized green synthesized iron nanoparticles: optimization, mechanism and DFT insights. *Journal of Environmental Chemical Engineering* 13(4):117350
[47] Lu Y, Zeng H, Lin H, Liang Y, Feng M, et al. 2024. Synergistic removal performance and mechanism of Cd(II) and As(III) from irrigation water by iron sulfide-based porous biochar. *Environmental Science and Pollution Research* 31(8):11591–11604
[48] Hu X, Ding ZH, Zimmerman AR, Wang S, Gao B. 2015. Batch and column sorption of arsenic onto iron-impregnated biochar synthesized through hydrolysis. *Water Research* 68:206–216
[49] Nguyen DK, Ly-Tran QB, Dinh VP, Duong BN, Nguyen TPT, et al. 2024. Adsorption mechanism of aqueous Cr(vi) by Vietnamese corncob biochar: a spectroscopic study. *RSC Advances* 14(53):39205–39218
[50] Tran TK, Huynh L, Nguyen HL, Nguyen MK, Lin C, et al. 2024. Applications of engineered biochar in remediation of heavy metal(loid)s pollution from wastewater: current perspectives toward sustainable development goals. *Science of The Total Environment* 926:171859
[51] Cato E, Rossi A, Scherrer NC, Ferreira ESB. 2018. An XPS study into sulphur speciation in blue and green ultramarine. *Journal of Cultural Heritage* 29:30–35
[52] Zhang J, Huang D, Shao J, Zhang X, Zhang S, et al. 2022. A new nitrogen-enriched biochar modified by ZIF-8 grafting and annealing for enhancing CO_2 adsorption. *Fuel Processing Technology* 231:107250
[53] Ahmed MMM, Liao CH, Liu YT, Venkatesan S, Hsieh YC, et al. 2024. Sulfur-functionalized rice straw biochar for enhanced cadmium sorption: spectroscopic, kinetic and computational insights. *Journal of Cleaner Production* 484:144267
[54] Meng Z, Wu J, Huang S, Xin L, Zhao Q. 2024. Competitive adsorption behaviors and mechanisms of Cd, Ni, and Cu by biochar when coexisting with microplastics under single, binary, and ternary systems. *Science of The Total Environment* 913:169524
[55] Teng D, Zhang B, Xu G, Wang B, Mao K, et al. 2020. Efficient removal of Cd(II) from aqueous solution by pinecone biochar: sorption performance and governing mechanisms. *Environmental Pollution* 265:115001